

AD-A152 216

A STUDY OF COMPUTATIONAL TECHNIQUES FOR NONCANONICAL
MICROSTRIP ANTENNAS AND ARRAYS(U) GEORGIA INST OF TECH
ATLANTA ENGINEERING EXPERIMENT STATION J J WANG JAN 85
RADC-TR-85-9 F/G 9/5

1/1

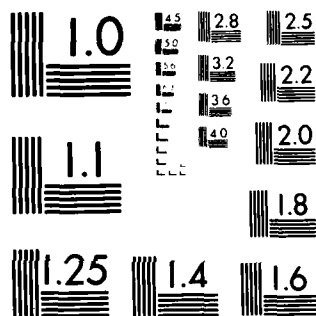
UNCLASSIFIED

NL

END

1/1

2/1



MICROCOPY RESOLUTION TEST CHART
NATIONAL BUREAU OF STANDARDS-1963-A

RADC-TR-85-9
Final Technical Report
January 1985



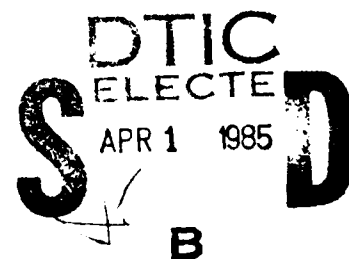
(4)

A STUDY OF COMPUTATIONAL TECHNIQUES FOR NONCANONICAL MICROSTRIP ANTENNAS AND ARRAYS

Georgia Institute of Technology

J. J. H. Wang

APPROVED FOR PUBLIC RELEASE; DISTRIBUTION UNLIMITED



ROME AIR DEVELOPMENT CENTER
Air Force Systems Command
Griffiss Air Force Base, NY 13441-5700

85 03 10 201

AD-A152 216

DTIC FILE COPY

This report has been reviewed by the RADC Public Affairs Office (PA) and is releasable to the National Technical Information Service (NTIS). At NTIS it will be releasable to the general public including foreign nations.

RADC-TR-85-9 has been reviewed and is approved for publication.

APPROVED:



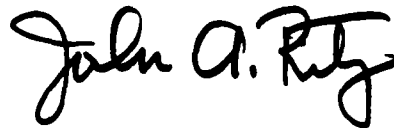
CHARLES J. DRANE
Project Engineer

APPROVED:



AXLAN C. SCHELL
Chief, Electromagnetic Sciences Division

FOR THE COMMANDER:



JOHN A. RITZ
Acting Chief, Plans Office

If your address has changed or if you wish to be removed from the RADC mailing list, or if the addressee is no longer employed by your organization, please notify RADC (EEAA) Hanscom AFB MA 01731. This will assist us in maintaining a current mailing list.

Do not return copies of this report unless contractual obligations or notices on a specific document requires that it be returned.

UNCLASSIFIED

SECURITY CLASSIFICATION OF THIS PAGE

AD-A152216

REPORT DOCUMENTATION PAGE

1a. REPORT SECURITY CLASSIFICATION UNCLASSIFIED		1b. RESTRICTIVE MARKINGS N/A	
2a. SECURITY CLASSIFICATION AUTHORITY N/A		3. DISTRIBUTION/AVAILABILITY OF REPORT Approved for public release; distribution unlimited	
2b. DECLASSIFICATION/DOWNGRADING SCHEDULE N/A			
4. PERFORMING ORGANIZATION REPORT NUMBER(S) N/A		5. MONITORING ORGANIZATION REPORT NUMBER(S) RADC-TR-85-9	
6a. NAME OF PERFORMING ORGANIZATION Georgia Institute of Technology	6b. OFFICE SYMBOL (If applicable)	7a. NAME OF MONITORING ORGANIZATION Rome Air Development Center (EEAA)	
6c. ADDRESS (City, State and ZIP Code) Engineering Experiment Station Atlanta, GA 30332		7b. ADDRESS (City, State and ZIP Code) Hanscom AFB MA 01731	
8a. NAME OF FUNDING/SPONSORING ORGANIZATION Rome Air Development Center	8b. OFFICE SYMBOL (If applicable) EEAA	9. PROCUREMENT INSTRUMENT IDENTIFICATION NUMBER F19628-81-K-0049	
6c. ADDRESS (City, State and ZIP Code) Hanscom AFB MA 01731		10. SOURCE OF FUNDING NOS.	
		PROGRAM ELEMENT NO 61102F	TASK NO 13
		PROJECT NO 2305	WORK UNIT NO 12
11. TITLE (Include Security Classification) ANALYSIS OF COMPUTATIONAL TECHNIQUES FOR NONCANONICAL MICROSTRIP ANTENNAS AND ARRAYS			
12. PERSONAL AUTHOR(S) J. L. M. M.			
13a. TYPE OF REPORT Final	13b. TIME COVERED FROM Aug 81 TO Nov 83	14. DATE OF REPORT (Yr., Mo., Day) January 1985	15. PAGE COUNT 58
16. SUPPLEMENTARY NOTATION N/A			
17. COSATI CODES		18. SUBJECT TERMS (Continue on reverse if necessary and identify by block number)	
FIELD	GROUP	Stratified media	
		Fast Fourier Transform (FFT)	
		Numerical Analysis	
19. ABSTRACT (Continue on reverse if necessary and identify by block number) Three computer tasks were performed on the analyses of microstrip antennas and arrays with noncanonical patch shapes. All three efforts include ultimately the development of computer programs for the analyses of a broad class of antenna configurations. The first task, which was intended to provide a basis for microstrip antenna analysis, was the development of a general numerical method for the analysis of an arbitrary Hertzian dipole in general stratified media. The Hertzian dipole can be vertical or horizontal, electric or magnetic. The media is a multi-layer with arbitrary layer thicknesses, and arbitrary dielectric constants. The second task reported here is the development of a computer algorithm for microstrip antennas in terms of an equivalent horizontal magnetic current along the periphery of the patch. The complex distribution of this magnetic current is determined by requiring that the radiated field on the patch surface vanish. Although numerical convergence was not achieved in the course of this research, this technique is considered highly promising (over)			
20. DISTRIBUTION/AVAILABILITY OF ABSTRACT UNCLASSIFIED UNLIMITED <input checked="" type="checkbox"/> SAME AS RPT. <input type="checkbox"/> DTIC USERS <input type="checkbox"/>		21. ABSTRACT SECURITY CLASSIFICATION UNCLASSIFIED	
22a. NAME OF RESPONSIBLE INDIVIDUAL Charles E. Deane		22b. TELEPHONE NUMBER (Include Area Code) (315) 861-2051	22c. OFFICE SYMBOL RADC (EEAA)

UNCLASSIFIED

SECURITY CLASSIFICATION OF THIS PAGE

and continued research is highly recommended.

Research on microstrip arrays was conducted for diode-switched microstrip panels with a radome cover. A moment method approach was taken with the aperture expanded in terms of exponential basis functions and a single mode in the diode-gap region. The computer program developed was checked against known data for the reflection and transmission of the basic sandwiched screen structure.

Application of these techniques can be found not only in microstrip antenna and arrays, but also in integrated circuits and geophysical sciences. 2.

UNCLASSIFIED

SECURITY CLASSIFICATION OF THIS PAGE

PREFACE

The research of this contract (F19628-81-K-0049) was carried out in the Electromagnetic Effectiveness Division of the Electronics and Computer Systems Laboratory of the Engineering Experiment Station at the Georgia Institute of Technology, Atlanta, Georgia 30332. This program was designated at Georgia Tech as Project A-3023 and Dr. Johnson J. H. Wang served as the Project Director. This Final Report covers the work which was performed from August 1981 to November 1983.



Approved For	✓
Special Agent	
Code	
Signature	
A-1	

SUMMARY

The objective of this program is to investigate new analytical/numerical techniques for microstrip antennas and arrays of noncanonical patch geometries. Antenna performance improvements, such as frequency band broadening and dual-frequency operations, are the ultimate goal in this investigation.

In the course of this research, a computer program for the radiation of an arbitrary Hertzian dipole in a general stratified multilayer medium was developed. Although the original intention was for application to microstrip antennas, this algorithm was later found to be applicable to a broad class of integrated circuits, geophysical problems, etc.

The analysis of microstrip antennas was focused on the development of a model of equivalent magnetic current along the periphery of the microstrip patch. This is a new technique derived from a similar approach in dealing with microstrip circuits of arbitrary shapes. Although numerical convergence problems presently exist, this approach appears very attractive for noncanonical microstrip antennas. Continued research in this approach is highly recommended.

Research in microstrip arrays was conducted for diode-switched microstrip panels sandwiched by dielectric layers. A moment method approach was taken with the aperture expanded in terms of exponential basis functions and a single mode in the diode-gap region. The computer program developed in this research was checked against known data for the reflection and transmission of sandwiched screen structures.

All of the three techniques investigated are promising approaches to treat microstrip antennas and arrays. It is recommended that substantial efforts be devoted to extend and approve the techniques. These future efforts should lead to progress in microstrip antenna technology as well as geophysics and integrated circuits.

TABLE OF CONTENTS

<u>Section</u>	<u>Page</u>
I. INTRODUCTION.	1
II. APPLICATION OF HERTZIAN DIPOLE ANALYSIS TO MICROSTRIP ANTENNAS.	3
A. Introduction.	3
B. Method of Replacing the Microstrip Patch by an Equivalent Current Sheet.	5
C. Solution in Terms of Peripheral Magnetic Current.	7
III. ANALYSIS OF A MICROSTRIP ARRAY.	13
A. Introduction.	13
B. Formulation of the Approach	17
C. Moment Method Solution.	21
D. Numerical Computation	24
IV. CONCLUSIONS AND RECOMMENDATIONS	35
V. REFERENCES.	37
 <u>Appendix</u>	
A. SOME DEFINITIONS AND RELATIONSHIPS USED IN SECTION III	41

LIST OF FIGURES

<u>Figure</u>		<u>Page</u>
1.	Top and front views of a general microstrip antenna with its feed circuits denoted by dashed lines	4
2.	Replacing the conducting patch by a current sheet \underline{J}_s .	6
3.	Peripheral electric field \underline{E}_s perpendicular to patch surface.	8
4.	An equivalent peripheral magnetic current model producing the same exterior fields as a microstrip antenna.	10
5.	Segmentation of the periphery of a microstrip antenna of arbitrary geometry.	11
6.	A diode-switched slot-array panel.	14
7.	A diode-switched strip array panel	15
8.	An element of a diode-switched slot array sandwiched by two dielectric layers	16
9.	Unit cell configuration and field distribution in the gap region D.	22
10.	Convergence test for the magnitude of the reflection coefficient for the case of Table III	29
11.	Convergence test for the phase of the reflection coefficient for the case of Table III	30
12.	Comparison between the present transmission computation (in triangles and circles) and those by Lee (solid lines) for the case of $A = B = 0.4$, $2d_a = 2d_b = 0.2A$, $t_1 = t_2 = 0.1$, $d_g = 0$ (all in wavelengths) and $\epsilon_{1r} = \epsilon_{2r}$ with TM incidence	31
13.	Comparison of the amplitude and phase of the TM transmission coefficient computed by Lee (in lines) and in this research (in triangles and circles) for the case of of Figure 12.	32

LIST OF TABLES

<u>Table</u>		<u>Page</u>
I.	COMPARISON FOR THE REFLECTION COEFFICIENT COMPUTATION FOR THE CASE OF $d_a = d_b = d_g = 0$ (SCREEN ALSO) AND $A = 0.2$, $B = 0$, $t = t_2 = 0.1$ (ALL IN WAVE- LENGTHS) $\epsilon_{r1} = \epsilon_{r2} = 2.5$	25
II.	COMPARISON FOR THE REFLECTION COEFFICIENT COMPUTATION FOR THE CASE OF $A = B = 0.2$, $d_b = d_g = 0$, $d_a = 0.05$, $t_1 = t_2 = 0.1$ (ALL IN WAVELENGTHS), $\epsilon_{r1} = \epsilon_{r2} = 1$. . .	27
III.	COMPARISON FOR THE REFLECTION COEFFICIENT COMPUTATION FOR THE CASE OF $A = B = 0.2$, $d_b = d_g = 0$, $d_a = 0.5$, $t_1 = t_2 = 0.1$ (ALL IN WAVELENGTHS), $\epsilon_{r1} = \epsilon_{r2} = 2.5$. . .	28

SECTION I

INTRODUCTION

The requirement for low-profile antennas with low fabrication costs has led to the recent interest in microstrip antennas. However, microstrip antennas have been found to be limited in their performance, especially regarding their typically narrow bandwidth of one to six percent. A theoretical investigation of noncanonical antennas appears promising in developing antennas of higher performances, as suggested in several experimental studies. In this study, techniques for analyzing microstrip antennas and arrays were investigated in order to develop computer algorithms for noncanonical patch shapes.

Three major accomplishments are reported in the following sections. A general numerical method for analyzing the radiation of an arbitrary Hertzian dipole in multi-layer stratified media was developed. Both the number of layers and their thicknesses and complex dielectric constants can be arbitrarily designated. The Hertzian dipole can be vertical or horizontal, electric or magnetic. The computational method was developed as a basis for the microstrip antenna analysis. However, its application was later found to be quite broad, including geophysical problems and integrated circuits.

The method of analysis for the microstrip antenna developed in this research is based on the representation of fields in terms of an equivalent horizontal magnetic current along the periphery of the microstrip patch. This method is particularly attractive for patches of arbitrary shapes. An integral equation in terms of equivalent peripheral magnetic current was derived and solved by the method of moments. Although the numerical data do not show the expected convergence behavior, the basic formulation and computer algorithm represent a highly promising approach which should provide a powerful tool for the analysis of noncanonical microstrip antennas when fully developed.

Analysis of microstrip diode switched arrays is a difficult problem for which little research has been performed. In this research, a moment method computer program was developed for a simple diode-switched monolithic slot (or strip) array. This program has been tested against data for a screen structure which have been presented in the literature.

These three major accomplishments represent progress in geophysical science stratified media problems and integrated circuits as well as the intended microstrip antenna and array analyses. All of the analyses involve new and useful numerical techniques which need further improvement for full fruition.

SECTION II

APPLICATION OF HERTZIAN DIPOLE ANALYSIS TO MICROSTRIP ANTENNAS

A. Introduction

A general microstrip antenna is depicted in Figure 1. The feeds, shown in dotted lines, can be either a probe feed or an end feed. In general, the end feed is preferred because it is simple to construct. Both the geometry of the microstrip patch and the location and type of feed are parameters determining the characteristics of the microstrip antenna. Current microstrip antenna technology, which has been extensively reviewed in an IEEE Transactions on Antennas and Propagation Special Issue [1] and two reference books [2,3], does not have analytical methods suitable for patches with noncanonical shapes.

The study of microstrip antenna (excluding arrays) technology has progressed from rectangular patches [4,5] to circular [6], elliptical [7,8], and triangular [5] patches, etc. With a new geometry, there is usually a new set of performance characteristics that represent an improvement over existing designs and may even find different new applications. However, as summarized by Carver and Mink [9], the microstrip antenna has typical bandwidths from one to six percent. Larger bandwidths, which may be achieved by increased substrate thickness or patch size, are often impractical. Kernweis and McIlverma [10,11] discovered that microstrip antennas could operate at dual frequencies if radial conducting strips were added to the patch.

The method of analysis for microstrip antennas is typically a technique highly dependent on the geometry of the patch. In fact, it deals as a rule microstrip patches with canonical shapes conforming to the several existing coordinate systems. Some efforts were made with limited success to apply the wire-grid method [12] and the finite-element technique [13] for patches of generalized shapes.

In the present analysis, we begin with the analysis of the fields due to an arbitrary Hertzian dipole in an arbitrary stratified medium. This approach is in essence similar to the Green's functions formulation such as that of Cavaleante, et al [14]. The numerical analysis techniques involved in this approach have been reported in the Interim Report [15] and are being

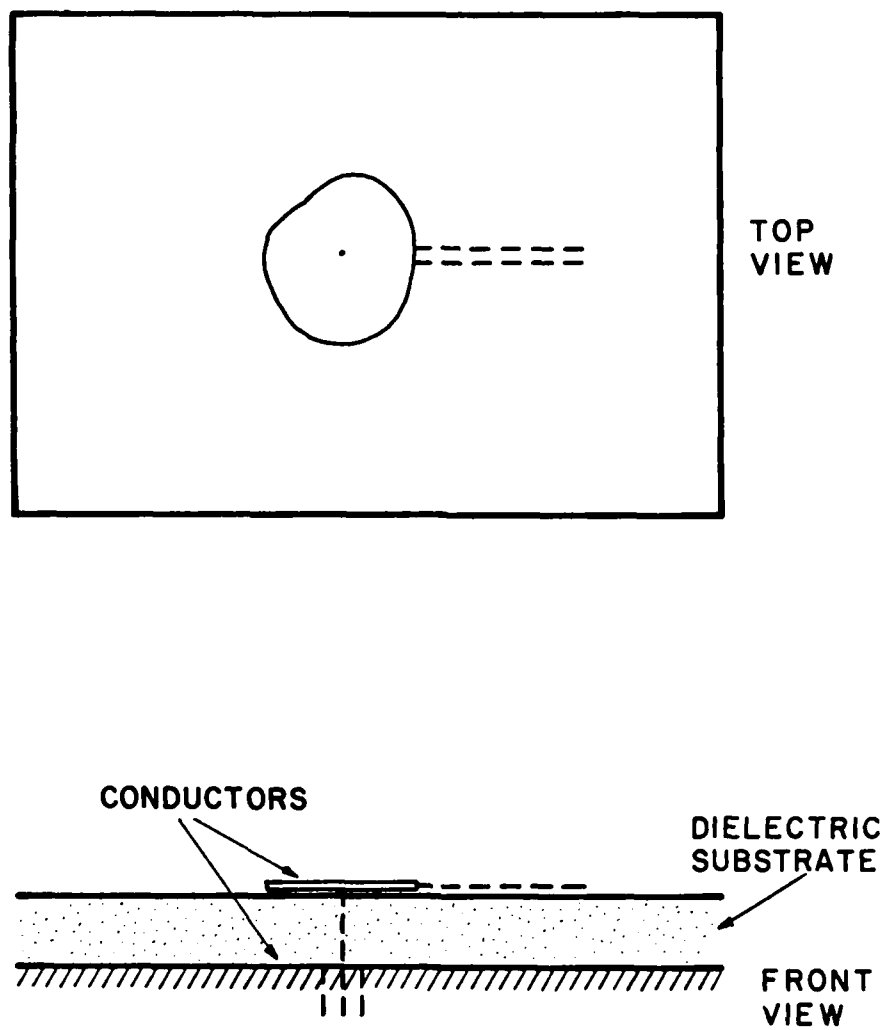


Figure 1. Top and front views of a general microstrip antenna with its feed circuits denoted by dashed lines.

formally published [16].

Two methods were studied in this research to analyze microstrip antennas, using the Hertzian dipole radiation as a building block. One is to replace the conducting microstrip patch by a sheet of equivalent surface current. The other is to formulate the problem in terms of the peripheral electrical fields of the patch. These are discussed as follows.

B. Method of Replacing the Microstrip Patch by an Equivalent Current Sheet

The conducting microstrip patch can be replaced by a sheet of current density \underline{J}_s , as shown in Figure 9. This is accomplished by using the surface equivalence theorem on the patch surfaces and then allowing the thickness of the patch to approach zero. The vertical \underline{J} symbolizes a probe feed. For an end-fed patch the excitation current should be horizontally directed.

The surface patch technique [17] can be employed to solve this boundary value problem. An electric field integral equation based on the boundary condition

$$\hat{n} \times (\underline{E}^i + \underline{E}^s) = 0 \text{ on the microstrip patch} \quad (1)$$

can be written. In Equation (1), \underline{E}^i is the field due to the excitation probe, \hat{n} is a unit normal to the patch, and \underline{E}^s is the electric field due to the equivalent surface current \underline{J}_s .

It is necessary to point out that the field at the source point contains a singular integrand, as can be seen in the field equations in Reference 15 used to compute the tangential field. It appears that the singularity is of the $1/\sqrt{r}$ type. No attempt was made to deal with this problem directly. Instead, the testing is performed slightly away from the source point which is the technique used by Richmond [18] and Harrington [19] in wire antenna analyses.

Another difficulty is due to the fact that the source and field points have the same z coordinates. This can be dealt with by choosing a small yet numerically acceptable difference between the z coordinates of the source and the field.

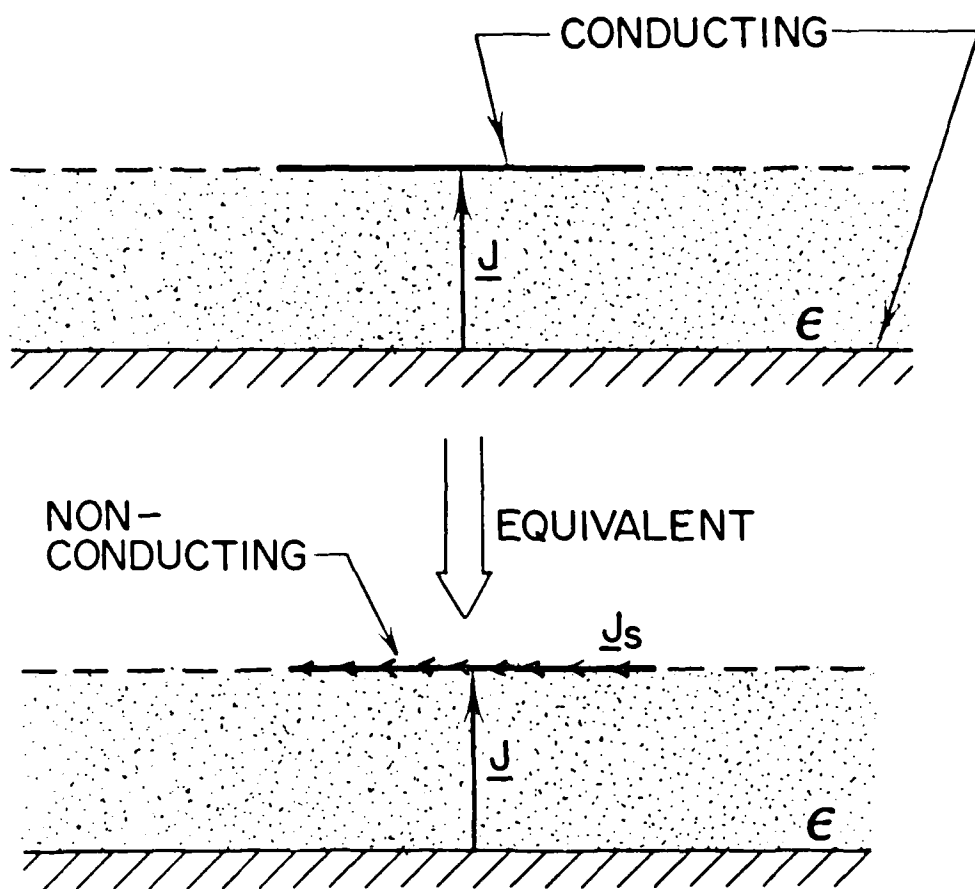


Figure 2. Replacing the conducting patch by a current sheet \underline{J}_s .

This type of point-matching method was applied to microstrip problems by Farrar and Adams [20] to calculate the capacitances of a patch and the gap between two patches. Their work was for a much simpler static model with little direct relevance to the antenna problem, which requires a full solution of the time-harmonic fields. However, examination of their work in comparison with the present approach indicated that development of an algorithm in the present approach would be impractical and difficult. In addition, their work, as well as others' [21-23], led to an awareness that the peripheral magnetic current plays a predominant role in the physics involved in microstrip structures. While earlier work addresses only circuit (interior) problems, the method of Okoshi [21] has direct implication to antenna problems. The equivalent electric current sheet method was thus abandoned in its early stage of development.

C. Solution in Terms of Peripheral Magnetic Current

The majority of analyses on microstrip structures take advantage of the fact that the substrates are electrically thin. As a result, the fields in the region between the patch and the ground plane contain primarily vertical E (perpendicular to the ground plane) and horizontal H fields. As shown in Figure 3, the fields in this region are also quite independent of the z coordinate. At the edge of the microstrip, current on the patch normal to the edge must vanish as required by the continuity of current. As a result, the tangential component of H field along the edge is negligible. Thus, the peripheral slot can be represented by an equivalent magnetic current $\hat{n} \times \underline{E}_s$, as shown in Figure 3, where \hat{n} is a unit vector normal to the peripheral surfaces (\hat{n} is always perpendicular to z), and \underline{E}_s is the total electric field on s given by

$$\underline{E}_s \cong E_z \hat{z} . \quad (2)$$

In this approach, \underline{E}_s , or the equivalent magnetic current $\hat{n} \times \underline{E}_s$, is the crux of the problem. This model has been extensively reported in the literature in conjunction with other numerical techniques for microstrip circuit problems. For microstrip antennas, however, it was primarily used in the approximate computation of the far-zone fields. It is, therefore, a

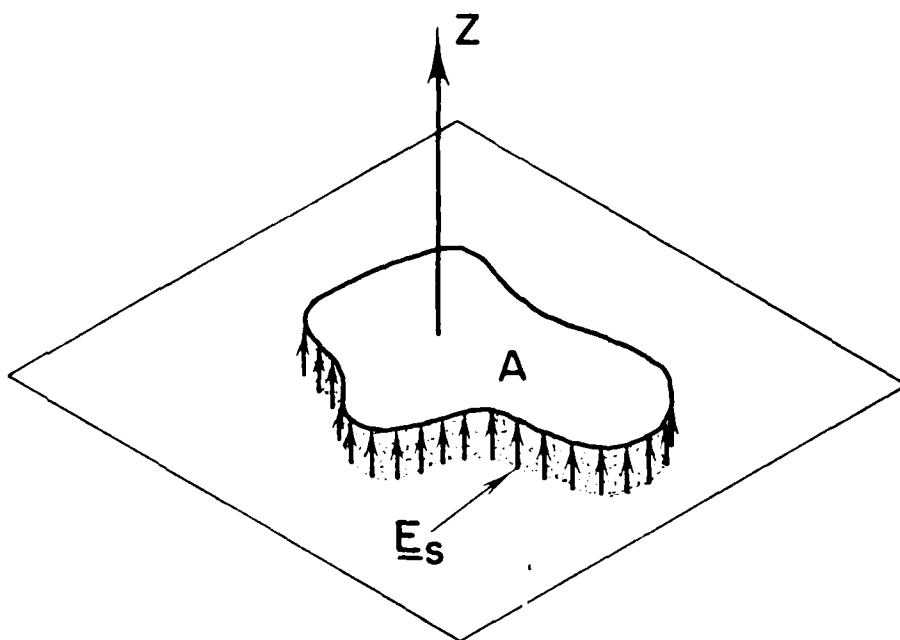


Figure 3. Peripheral electric field \underline{E}_s perpendicular to patch surface.

natural step to expand this technique, which has been very successful in dealing with microstrip circuits, to microstrip antennas.

The approach of Okoshi and Miyoshi [21] appeared to be particularly suitable to antenna problems because it deals directly with the exterior problem with an integral equation. Consequently, Gupta visualized the advantage of this approach and applied it to microstrip antennas [24-27].

An additional advantage of the peripheral magnetic current method is its adaptability to the microstrip antennas with radial conducting strips for dual frequency operation invented by McIlvanna and Kerneis [10,11]. Effects of the radial conducting strips can be treated as a circuit problem in which the impedance of the strip is computed with closed-form analytical formulas.

A new approach was taken in this research. The exterior field of a microstrip antenna is represented by a magnetic current over the peripheral opening and a conducting surface enclosing the antenna region as shown in Figure 4, [2,13]. This model follows directly from the equivalence principle and the uniqueness principle [28, p. 108].

As shown in Figure 5, we can now expand \underline{M}_s into a peripheral distribution along s , the periphery, as

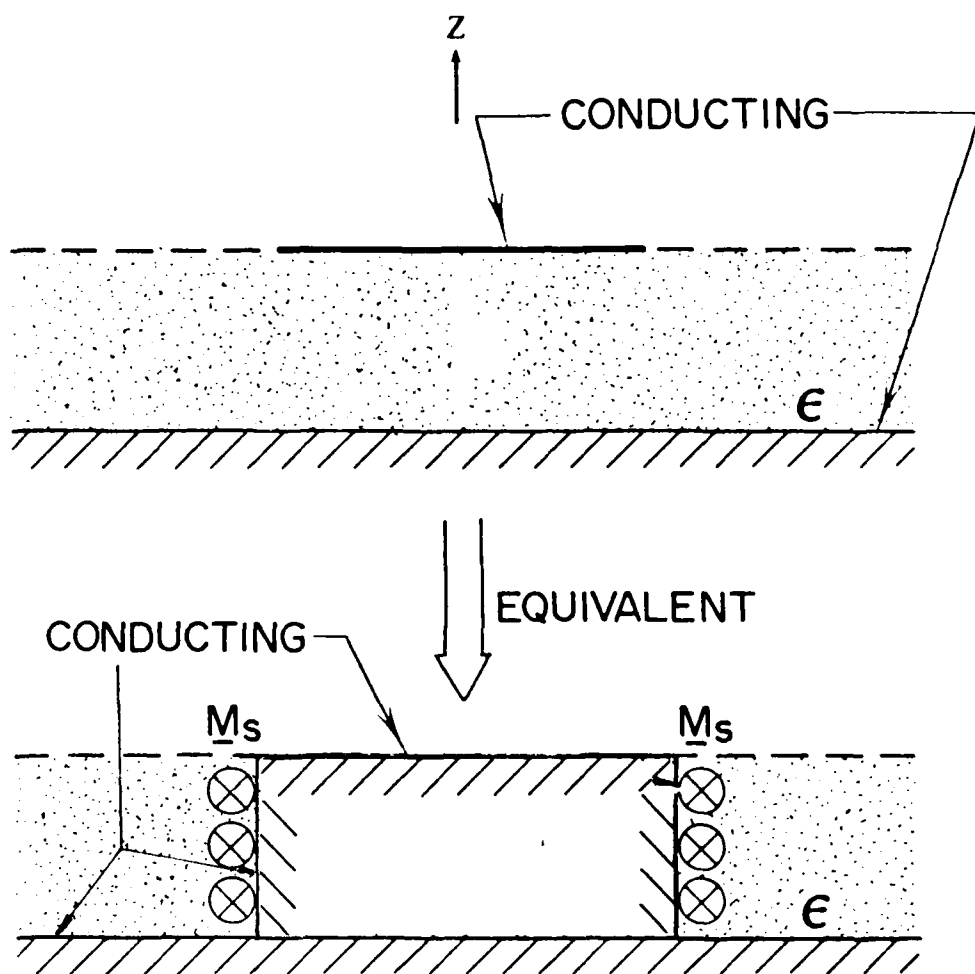
$$\underline{M}_s = \sum_{n=1}^N \underline{M}_{sn} P(S_n), \quad (3)$$

where $P(S_n)$ is a pulse function such that,

$$\begin{aligned} P(S_n) &= 1 && \text{if } S_n > S > S_{n+1}, \\ &= 0 && \text{elsewhere.} \end{aligned} \quad (4)$$

\underline{M}_{sn} is a horizontal magnetic current element that produces fields as if the microstrip antenna region did not exist. That is, \underline{M}_{sn} produces fields in the substrate over the ground plane -- a problem treated extensively in the preceding section.

The presence of the microstrip antenna region, represented by a conducting pill box, in Figure 4 requires that the amplitude and phase of all the \underline{M}_{sn} 's be adjusted so that the tangential E fields vanish on the top and the side (periphery) of the pill box. Note that fields due to each \underline{M}_{sn}



$$\underline{M}_s = \underline{E}_s \times \hat{n} = E_{sz} \hat{z} \times \hat{n} = E_{sz} \hat{t}$$

Figure 4. An equivalent peripheral magnetic current model producing the same exterior fields as a microstrip antenna.

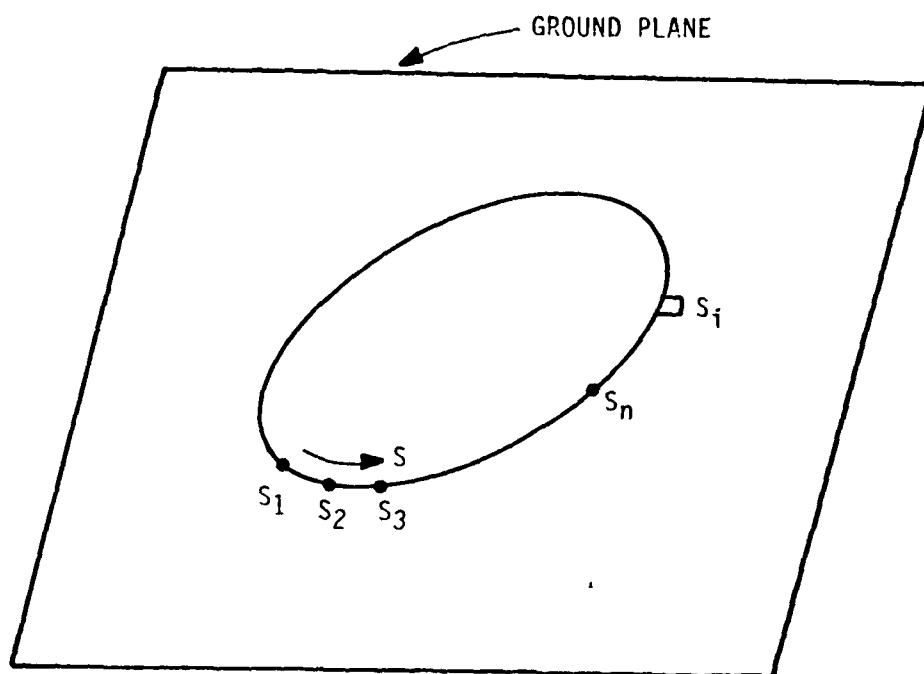


Figure 5. Segmentation of the periphery of a microstrip antenna of arbitrary geometry.

satisfy, by definition, Maxwell's equations and the boundary conditions outside (but not on) the pill box.

Note that in this case it is not necessary to enforce the boundary condition for tangential H even though in general a boundary condition for tangential H is also required. This is due to the fact that in the present formulation, tangential H on the dielectric interface due to each \underline{M}_{sn} is by definition already continuous at the interface. Thus an integral equation of the form

$$\oint (\underline{M}_s + \underline{M}_i) = 0 \quad (5)$$

on the microstrip patch can be written. \underline{M}_i is the end-fed excitation magnetic current of the microstrip antenna.

Physically, this formulation is similar to those of Okoshi and Gupta and their colleagues [21,24-27]. The integral equation is expressed in terms of the peripheral magnetic current and excitation current alone. This is a definite advantage in treating arbitrarily shaped patches and in particular, the antenna with radial conducting strips.

The present method can also be viewed as a modal or eigenfunction solution. All the possible modes of fields for the exterior and interior regions are those due to horizontal magnetic current elements at the periphery. The combined effect of the microstrip patch is that tangential E field vanishes on this microstrip patch of infinitesimal thickness. This approach is similar to the modal expansion techniques used extensively in waveguide discontinuities and array antennas.

A computer program based on Equations (4) and (5) was written to solve the microstrip antenna problem by the method of moments [19]. However, a lack of anticipated numerical convergence was observed. During the exhaustive debugging stage, it became clear that new concepts and techniques were involved in this computer program which needed more debugging and investigation. This promising method in dealing with noncanonical microstrip antennas merits further extensive numerical exploration to bring it to fruition.

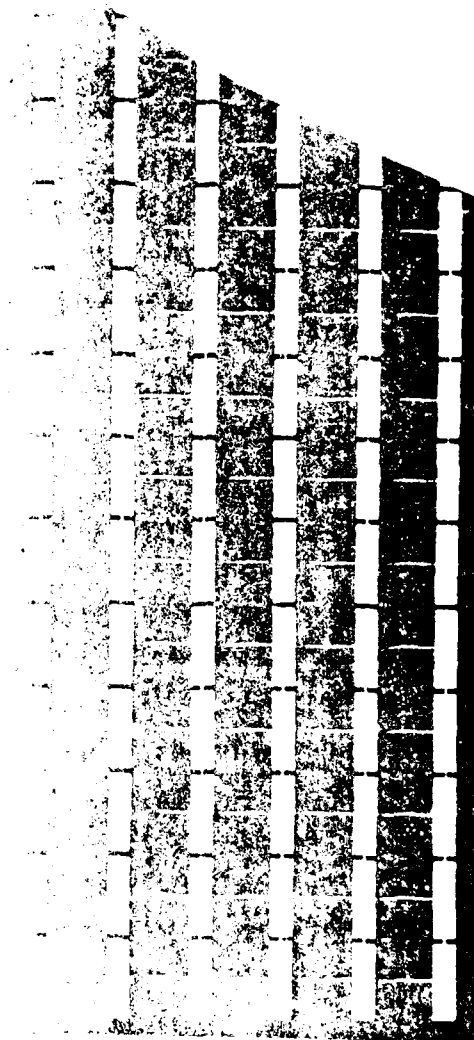
SECTION III

ANALYSIS OF A MICROSTRIP ARRAY

A. Introduction

The analysis of a microstrip array is a difficult problem. As a result, very little has been reported in this area even though other arrays such as waveguide and dipole arrays have been extensively studied. Thorough reviews on microstrip arrays can be found in references 2 and 29. The difficulties in microstrip array analyses are primarily in the handling of the interaction in the feed region. Recently, Liu, et al [30] reported an analytical method which deals with the feed by approximating the vertical probe feeds with a continuous and uniform current sheet. Interestingly, they also broke up the analysis into two simpler ones by employing the equivalence principle -- a technique similar in many aspects to the peripheral magnetic current method described in the preceding section. Since future development of phased arrays will probably emphasize monolithic and multilayer structures [29], emphasis in this research was on the PIN diode switched structure shown in Figures 6 and 7. The tiny gaps, each about 10 mils wide, are connected with PIN diodes which are switched on and off at a low rate. The long thin slots in Figure 6 insulate the diode bias currents which flow through the conducting (black) surfaces. The slots (in white) are switched on and off with these diodes. Alternatively, conducting strips, instead of slots, can be designed to form a switching surface, as shown in Figure 7. It is expected that the techniques developed in treating these types of microstrip arrays will be useful for other similar microstrip arrays. Thus, a more general type of element slot configuration as shown in Figure 8 was chosen for the computer program input. The switching of the phase front for the reflected or transmitted wave, and thus the direction of the antenna beam, is accomplished by the individually switched PIN diodes.

There are two major analytic difficulties involved in the computation of scattering of this configuration; the complex geometry of the aperture and the effect of the diodes. Scattering of screen structures for rectangular and circular apertures (or plates) were treated by Chen [31,32] and Lee [33]. Analyses involving loading and other geometries were



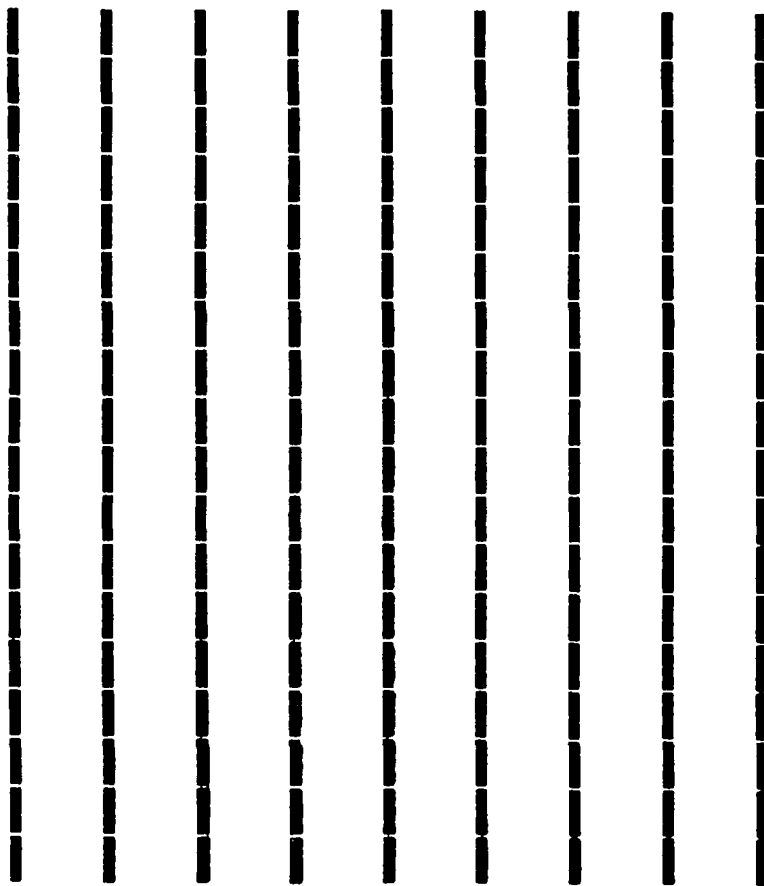


Figure 7. A diode-switched strip array panel.

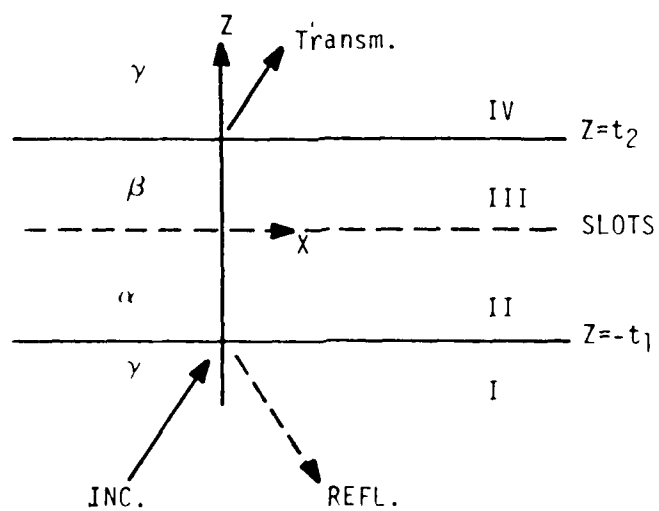
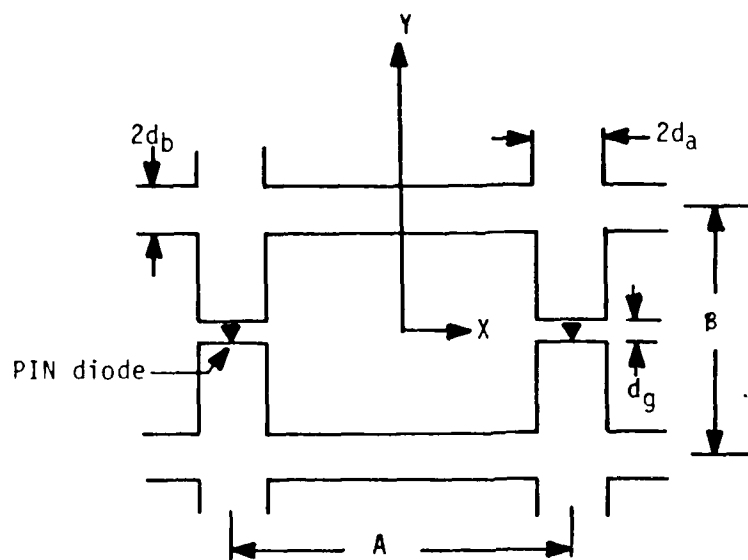


Figure 5. An element of a diode-switched slot array sandwiched by two dielectric layers.

conducted by Munk, et al [35] for thin slots and dipoles. Recent research in the Jerusalem-cross geometry has also been performed for thin crosses for which simple current distributions can be reasonably postulated [36-38].

In this research, the effects of loading and slot geometry are included -- the slot is not assumed to be thin. It is difficult to find a suitable set of basis functions to represent the unknown aperture field to obtain a numerical solution. Natural waveguide modes for this slot could be obtained in a manner similar to the ridged waveguide solutions by Montgomery [38]. However, the analysis would be very complex and this is why it has not yet been attempted. Another possible approach, which was chosen in this research, is to expand the unknown aperture fields in a set of orthogonal exponential basis functions. These exponential functions are closely related to the sinusoidal functions representing rectangular waveguide modes, but they are not as restrictive on the boundaries so that continuity at $X = A/2 - d_a$ is possible. However, difficulties are expected in this method in establishing criteria for relative convergence [39,40].

B. Formulation of the Approach

We begin by dividing the problem into the TE (transverse electric) and TM (transverse magnetic) cases. The incident wave for each case can be represented as

$$\underline{E}_e^i = \hat{\phi} (-jk_0 \sin\theta) A_e^i e^{-jk_0 \cdot \underline{r}} \quad \text{TE ,} \quad (6)$$

and

$$\underline{E}_m^i = \hat{\theta} (jk_0 \sin\theta) \eta_0 A_m^i e^{-jk_0 \cdot \underline{r}} \quad \text{TM ,} \quad (7)$$

where

$$\eta_0 = \sqrt{\mu_0/\epsilon_0} \quad , \quad (8a)$$

$$\underline{k}_0 = k_0 [\sin\theta \cos\phi \hat{x} + \sin\theta \sin\phi \hat{y} + \cos\theta \hat{z}] \quad , \quad (8b)$$

$$k_0 = \omega \sqrt{\epsilon_0 \mu_0} \quad , \quad (8c)$$

$$\underline{r} = r\hat{r} = x\hat{x} + y\hat{y} + z\hat{z} \quad , \quad (8d)$$

$$\hat{\theta} = \cos\theta \cos\phi \hat{x} + \cos\theta \sin\phi \hat{y} - \sin\theta \hat{z} \quad , \text{ and} \quad (8e)$$

$$\hat{\phi} = -\sin\phi \hat{x} + \cos\phi \hat{y} \quad . \quad (8f)$$

It is possible to represent fields in all four regions, I through IV in Figure 8, in terms of vector potential \underline{A} in each region [33]. For the incident wave,

$$\underline{A}_e^i = \hat{z} A_{ez}^i = \hat{z} A_e^i e^{-jk \cdot \underline{r}}, \text{ and} \quad (9a)$$

$$\underline{A}_m^i = \hat{z} A_{mz}^i = \hat{z} A_m^i e^{-jk \cdot \underline{r}}. \quad (9b)$$

We can write, for each region, the forward and backward propagating vector potentials as follows.

Region I

$$\begin{bmatrix} A_{ze}^l \\ A_{zm}^l \end{bmatrix} = \begin{bmatrix} A_{ze}^{lf} + A_{ze}^{lr} \\ A_{zm}^{lf} + A_{zm}^{lr} \end{bmatrix} = \sum_p \sum_q \begin{bmatrix} A_e^i \delta_p^o \delta_q^o \\ A_m^i \delta_p^o \delta_q^o \end{bmatrix} \psi_{pq}(x,y) e^{-j_1 pqz} \\ + \sum_p \sum_q \begin{bmatrix} A_{epq}^r \\ A_{mpq}^r \end{bmatrix} \psi_{pq}(x,y) e^{j_1 pqz} \quad (10)$$

Region II

$$\begin{bmatrix} A_{ze}^2 \\ A_{zm}^2 \end{bmatrix} = \begin{bmatrix} A_{ze}^{2f} + A_{ze}^{2r} \\ A_{zm}^{2f} + A_{zm}^{2r} \end{bmatrix} = \sum_p \sum_q \begin{bmatrix} A_{epq}^{2f} \\ A_{mpq}^{2f} \end{bmatrix} \psi_{pq}(x,y) e^{-j_2 pqz} \\ + \sum_p \sum_q \begin{bmatrix} A_{epq}^{2r} \\ A_{mpq}^{2r} \end{bmatrix} \psi_{pq}(x,y) e^{j_2 pqz} \quad (11)$$

Region III

$$\begin{bmatrix} A_{ze}^3 \\ A_{zm}^3 \end{bmatrix} = \begin{bmatrix} A_{ze}^{3f} + A_{ze}^{3r} \\ A_{zm}^{3f} + A_{zm}^{3r} \end{bmatrix} = \sum_p \sum_q \begin{bmatrix} A_{epq}^{3f} \\ A_{mpq}^{3f} \end{bmatrix} \psi_{pq}(x,y) e^{-j\beta_{pq}z} + \sum_p \sum_q \begin{bmatrix} A_{epq}^{3r} \\ A_{mpq}^{3r} \end{bmatrix} \psi_{pq}(x,y) e^{j\beta_{pq}z} \quad (12)$$

Region IV

$$\begin{bmatrix} A_{ze}^4 \\ A_{zm}^4 \end{bmatrix} = \begin{bmatrix} A_{ze}^{4f} + A_{ze}^{4r} \\ A_{zm}^{4f} + A_{zm}^{4r} \end{bmatrix} = \sum_p \sum_q \begin{bmatrix} A_{epq}^{4f} \\ A_{mpq}^{4f} \end{bmatrix} \psi_{pq}(x,y) e^{-j\gamma_{pq}z} \quad (13)$$

where the summations over p and q are actually truncated to $\pm P$ and $\pm Q$, and

$$\psi_{pq}(x,y) = (AB)^{-1/2} e^{-j(U_{po}x + V_{pq}y)}, \quad (14a)$$

$$U_{po} = 2\pi p/A + k_0 \sin\theta \cos\phi, \text{ and} \quad (14b)$$

$$V_{pq} = 2\pi q/B + k_0 \sin\theta \sin\phi. \quad (14c)$$

A pair of integral equations can be obtained by enforcing boundary conditions at the three dielectric interfaces. Let the electric field at the aperture region at $z = 0$ be

$$\underline{E}_{ap} = E_{ax} \hat{x} + E_{ay} \hat{y}, \quad (15)$$

The following two integral equations can be obtained by matching the E field at the boundary at $z = 0$,

$$\int_{\text{aper}} E_{ay} \psi_{pq}^* (x,y) dx dy = -j u_{po} \left[\delta_p^o \delta_q^o \rho_{pq}^{(1)} A_e^i + \rho_{pq}^{(2)} A_{epq}^r \right] + \frac{j v_{pq} \alpha_{pq}}{\omega \epsilon_1} \left[\delta_p^o \delta_q^o \bar{\sigma}_{pq}^{(1)} A_m^i + \bar{\sigma}_{pq}^{(2)} A_{mpq}^r \right], \quad (16)$$

and

$$\int_{\text{aper}} E_{ax} \psi_{pq}^* (x,y) dx dy = -j v_{po} \left[\delta_p^o \delta_q^o \rho_{pq}^{(1)} A_e^i + \rho_{pq}^{(2)} A_{epq}^r \right] + \frac{j u_{pq} \alpha_{pq}}{\omega \epsilon_1} \left[\delta_p^o \delta_q^o \bar{\sigma}_{pq}^{(1)} A_m^i + \bar{\sigma}_{pq}^{(2)} A_{mpq}^r \right], \quad (17)$$

for $p, q = 0, \pm 1, \pm 2, \dots (\pm, \pm Q)$,

where the integration is over the aperture of a unit cell at $z = 0$ and δ_p^o and δ_q^o are the Kronecker delta function and the coefficients α_{pq} , etc. are defined in the appendix. Although the derivation so far has been along the same path as that of Lee [33], there are nontrivial differences in the mathematical expressions derived. Thus, the detailed expressions are included in Appendix B for comparison.

Equations (16) and (17) contain too many unknowns. They can be further reduced by enforcing the boundary condition for H field at $z = 0$ and eliminating all the unknown A parameters according to the transmission relationships in the appendix. Thus, we have

$$\int_{\text{aper}} \begin{bmatrix} K_{xx} & K_{xy} \\ K_{yx} & K_{yy} \end{bmatrix} \begin{bmatrix} E_{ax}(x',y') \\ E_{ay}(x',y') \end{bmatrix} dx' dy' = \begin{bmatrix} J_e(x,y) \\ J_m(x,y) \end{bmatrix} \quad (18)$$

The explicit description of this integral equation is included in the appendix.

C. Moment Method Solution

The pair of integral Equation (18) can be solved by the well known method of moments. Two major difficulties are involved: the construction of suitable basis functions and the treatment of the relative convergence problem. We choose, for the unknown aperture fields, the following expansion:

$$\begin{aligned} E_{ax} &= \sum_{m=-M}^M \sum_{n=-N}^N A_{mn} \phi_{mn}(x,y) && \text{in region C ,} \\ &= 0 && \text{in region D ,} \end{aligned} \quad (19)$$

$$\begin{aligned} E_{ay} &= \sum_{m=-M}^M \sum_{n=-N}^N B_{mn} \phi_{mn}(x,y) && \text{in C ,} \\ &= E_{ay}^g = E_g e^{j(sx+wy)} \cos \{ [|x| - (A/2 - d_a)] \pi / (2g) \} && \text{in D ,} \end{aligned} \quad (20)$$

where C and D are regions of the aperture in the unit cell shown in Figure 9. g is the effective gap width and

$$\begin{aligned} g &= g_{on} \text{ when the diode is forward-biased , and} \\ &= g_{off} \text{ when the diode is reverse-biased .} \end{aligned} \quad (21)$$

The basis function ϕ_{mn} constitute an orthonormal set in region C if we choose

$$\phi_{mn}(x,y) = [(A - 2d_a)(B - 2d_b)]^{-1/2} e^{-j(U'_{po}x + V'_{pq}y)} \quad , \quad (22)$$

where

$$U'_{po} = 2p\pi / (A - 2d_a) + k_0 \sin\theta_0 \cos\phi_0 \quad , \text{ and} \quad (23)$$

$$V'_{pq} = 2q\pi / (B - 2d_b) + k_0 \sin\theta_0 \sin\phi_0 \quad .$$

The above expansion can also be set up in the following manner to show the orthogonality of the basis functions. We write

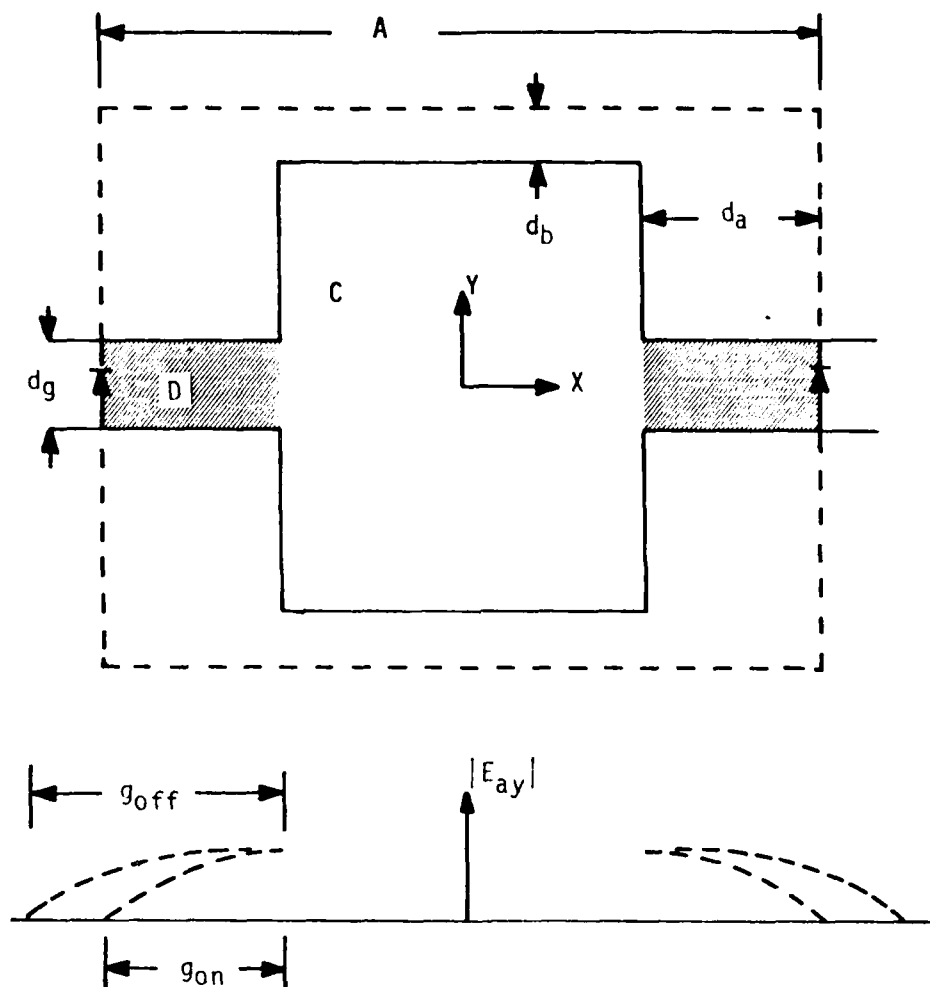


Figure 9. Unit cell configuration and field distribution in the gap region D.

$$E_{ax} = \sum_{m=-M}^M \sum_{n=-N}^N A_{mn} \phi_{mn}^x, \quad (24)$$

$$E_{ay} = \sum_{m=-M}^M \sum_{n=-N}^N B_{mn} \phi_{mn}^y, \quad (25)$$

where ,

$$\phi_{mn}^x = \phi_{mn} P_C, \quad \text{and} \quad (26)$$

$$\phi_{mn}^y = \phi_{mn} P_C + \delta_m^n \delta_{n+1}^N E_{ay}^g P_d. \quad (27)$$

P_C and P_d are pulse functions defined as ,

$$\begin{aligned} P_C &= 1 && \text{in } c, \\ &= 0 && \text{elsewhere.} \end{aligned} \quad (28)$$

The orthogonality among ϕ_{mn}^x and ϕ_{mn}^y is readily obvious since $P_C \cdot P_d = 0$. This is the subsectional expansion discussed in Reference 19 .

In addition to the integral Equation (18), we need two more equations to insure the continuity of tangential E fields at $x = \pm (A/2 - d_a)$ and $|y| < d_g/2$. Thus we add the following equations

$$\sum_{m=-M}^M \sum_{n=-N}^N B_{mn} \phi_{mn}^y (\pm [A/2 - d_a], 0) = E_{ay}^g (\pm [A/2 - d_a], 0) \quad (29)$$

The use of exponential functions to represent fields in Region c is advantageous in the present problem because it allows non-vanishing E_y at x

$= \pm(A/2-d_a)$ needed for the continuity of fields between regions C and D. However, the choice of the exponential function is not as efficient as waveguide modes in meeting the edge conditions at other conducting edges away from the gap.

Solution of Equations (18) and (29) was carried out by using the same relative convergence criteria established by Lee [33] for rectangular apertures. Thus, P and Q are first chosen based on an initial guess of the physical nature of the problem and the memory size of the computer. M and N are then chosen as

$$M_c = \left\lceil \frac{A-2d_a}{A} P \right\rceil, \text{ and} \quad (30)$$

$$N_c = \left\lceil \frac{B-2d_b}{B} Q \right\rceil,$$

where $\lceil a \rceil$ denotes the largest integer in a . As was pointed out in References 39 and 40, this choice of M and N for the particular P and Q leads to the most accurate results; larger M and N often yield poor results.

The effect of the gap is a reduction in the effective d_a in Equation (30). For arrays with small d_a , as often encountered in practice, the gap has little effect on M_c ; M_c can be chosen according to Equation (30) or with one additional mode.

D. Numerical Computation

A computer program was written to analyze the type of microstrip array shown in Figure 8 with emphasis on the strip type shown in Figure 1, which is the special case with $d_b = 0$. Testing and debugging of the program began with cases in which the metal screen was absent, that is, $d_a = d_b = 0$. The problem is the well-known reflection and transmission through a dielectric layer. Table I shows a comparison between this computation and the results of Lee (estimated from Figure 2 of Reference 35). The agreement can be considered extremely good since Lee's data were extracted from a figure by estimation. Note that there is a 180° difference between the phases of TE and TM reflection coefficient. This is

TABLE I

COMPARISON FOR THE REFLECTION COEFFICIENT COMPUTATION FOR THE
CASE OF $d_a = d_b = d_g = 0$ (SCREEN ALSO) AND $A = 0.2$, $B = 0$,
 $t_1 = t_2 = 0.1$ (ALL IN WAVELENGTHS) $\epsilon_{r1} = \epsilon_{r2} = 2.5$

ANGLE (deg)		TE		TM	
θ	ϕ	Amp.	phase (deg)	Amp.	phase (deg)
1°	0°	0.395 (0.395)	-130 (-130)	0.398 (0.395)	50 (50)
40°	0°	0.54 (0.54)	-137 (-137)	0.267 (0.267)	42 (42)

(): LEE (estimated)

due to the difference in sign in the incidence wave in Equations (6) and (7). To be a true reflection coefficient, 180° has to be added to the TM case.

Next we check the case in which $d_b = 0$ so that the screen becomes an array of parallel strips. The dielectric layers are chosen to be absent by letting $\epsilon_{r1} = \epsilon_{r2} = 1$. The computed results are again compared with those of Lee in Table II with excellent agreement. However, we noticed that the choice of M and N is essential to the accuracy of the results. For example, if we increase the number of M modes by choosing $M = M_c + 1$, ($M_c = 3$), the computed TM reflection coefficient becomes 0.122 at $\theta = 10^\circ$ and 0.0939 at $\theta = 40^\circ$, even though other computed results change very little. Thus, a 14% change in computed results is highly possible if the choice of modes is only slightly different. This is the well-known phenomenon of relative convergence. In the following, it will be shown that this remains to be a difficulty in the use of this computer program.

Next, we let $\epsilon_r = 2.5$ in the two dielectric layers in the case of Table II. The results are compared again with Lee's in Table III. Large discrepancies now appear, especially for the TE case. To examine whether this is due to a lack of relative convergence, we perform a convergence test and present the results in Figures 10 and 11 for the amplitude and phase of the reflection coefficient. As can be seen, the convergence is fairly good near M_c .

Recalling that the excellent agreement in Table II had not been reached until two printing errors in the input data described in the text of the paper were detected, it was conjectured that errors might exist also in the input data for the case in Table III. The discrepancy was thus believed to be due to differences in input data, not program bugs. To further illustrate this point, let us examine the case of a full screen in which $A=B=0.4$, $2d_a = 2d_b=0.2 \lambda$, $t_1=t_2=0.1$, $d_g=0$ (all in wavelengths), and $\epsilon_{r1} = \epsilon_{r2} = 2.5$. The total transmission coefficient (including the depolarized wave transmitted) in dB is computed in comparison with Lee's data in Figure 12. The incident wave is transverse magnetic with its incidence angles indicated. The agreement is quite good except at near $\theta=58^\circ$, where the present calculation has a sharper drop than that of Lee. An even more challenging case is shown in Figure 13, in which the computations of the amplitude and phase of the TM transmission coefficient

TABLE II

COMPARISON FOR THE REFLECTION COEFFICIENT COMPUTATION
 FOR THE CASE OF $A = B = 0.2$, $d_b = d_g = 0$, $d_a = 0.05$,
 $t_1 = t_2 = 0.1$ (ALL IN WAVELENGTHS), $t_{r1} = t_{r2} = 1$

ANGLE (deg)		TE		TM	
θ	ϕ	Amp.	phase (deg)	Amp.	phase (deg)
1°	0°	0.978	171	0.142	82
		(0.978)	(169)	(0.142)	(83)
40°	0°	0.992	173	0.110	84
		(0.990)	(173)	(0.112)	(84)

(): LEE (estimated)

TABLE III

COMPARISON FOR THE REFLECTION COEFFICIENT COMPUTATION
 FOR THE CASE OF $A = B = 0.2$, $d_b = d_g = 0$, $d_a = 0.5$,
 $t_1 = t_2 = 0.1$ (ALL IN WAVELENGTHS), $\epsilon_{r1} = \epsilon_{r2} = 2.5$

ANGLE (deg)		TE		TM	
θ	ϕ	Amp.	phase (deg)	Amp.	phase (deg)
1°	0°	0.948 (0.72)	145 (119)	0.543 (0.55)	41 (32)
40°	0°	0.963 (0.73)	151 (127)	0.436 (0.58)	31 (22)

(): LEE (estimated)

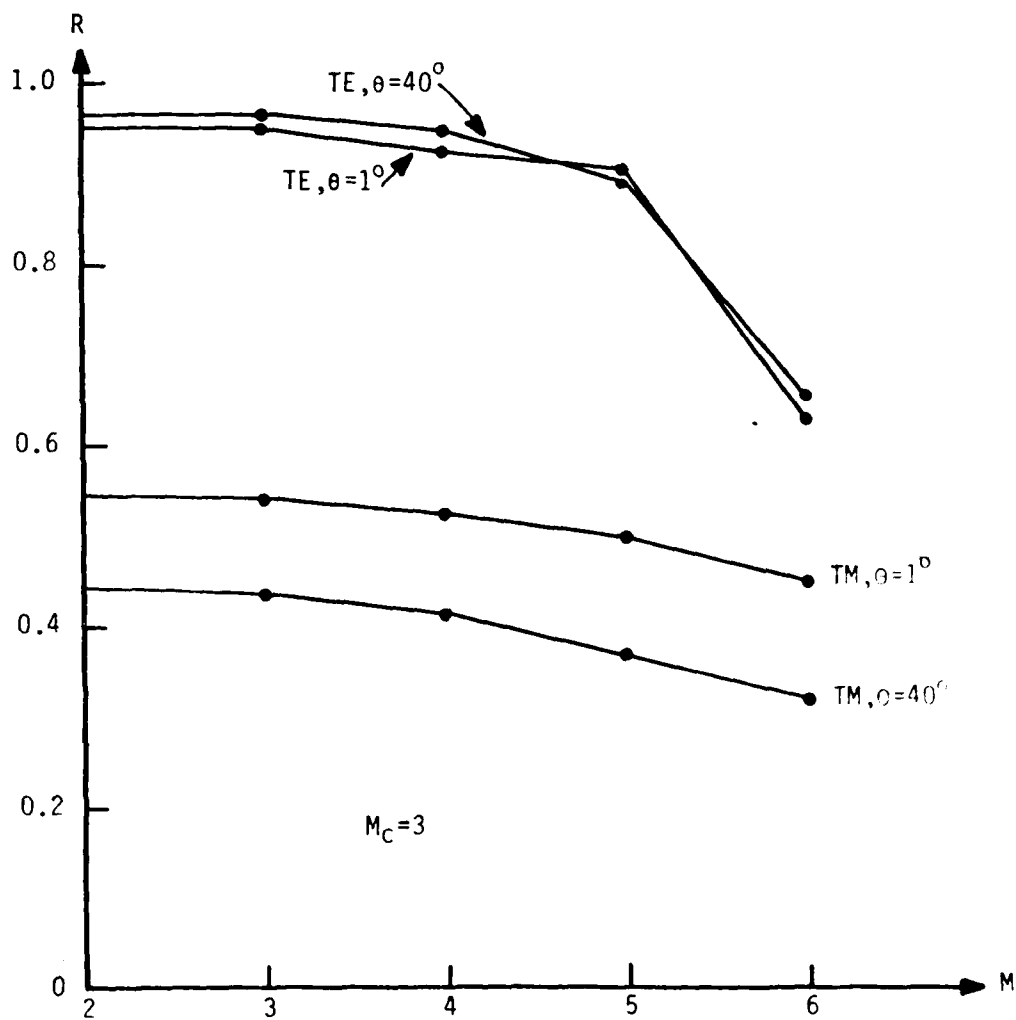


Figure 10. Convergence test for the magnitude of the reflection coefficient for the case of Table III.

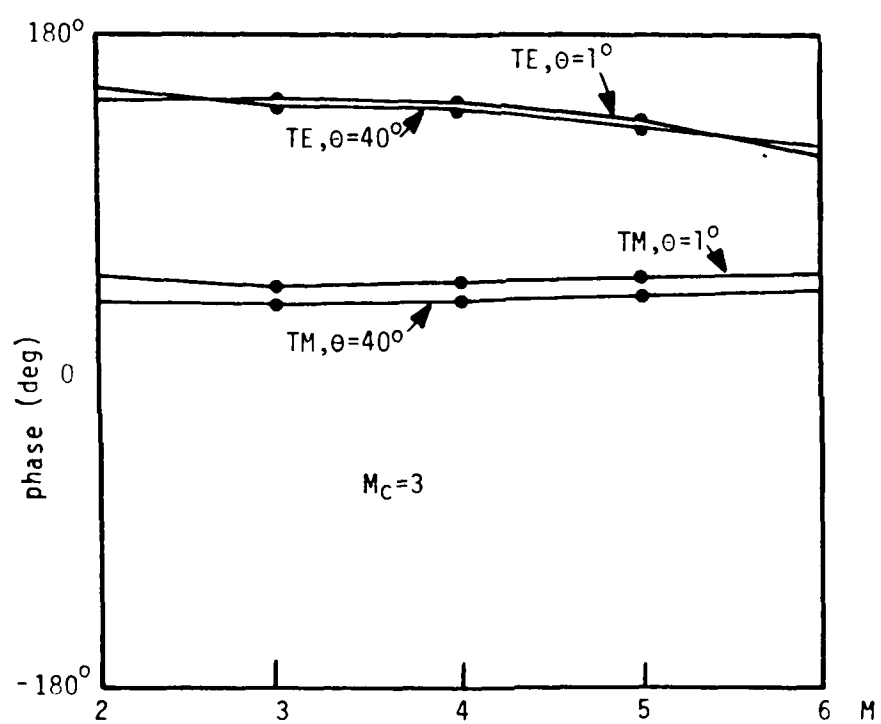


Figure 11. Convergence test for the phase of the reflection coefficient for the case of Table III.

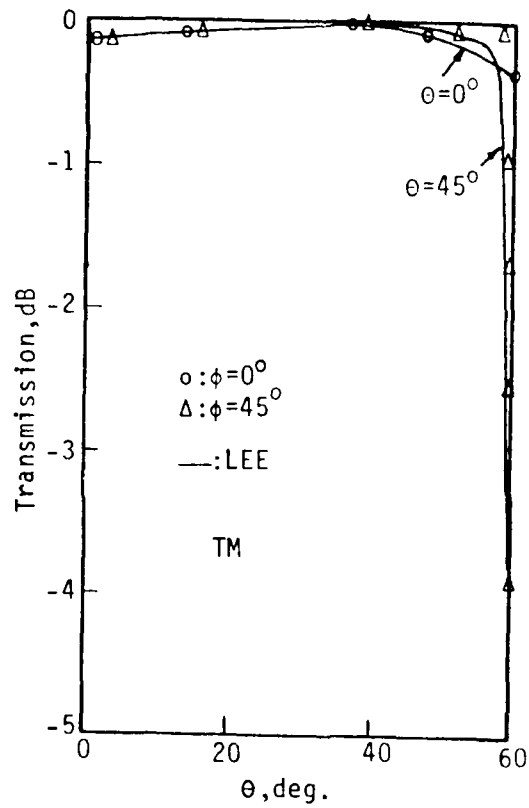


Figure 12 Comparison between the present transmission computation (in triangles and circles) and those by Lee (solid lines) for the case of $A = B = 0.4$, $2d_a = 2d_b = 0.2\lambda$, $t_1 = t_2 = 0.1$, $d_g = 0$ (all in wavelengths) and $\frac{d_a}{r} = \frac{d_b}{2r}$ with TM incidence.

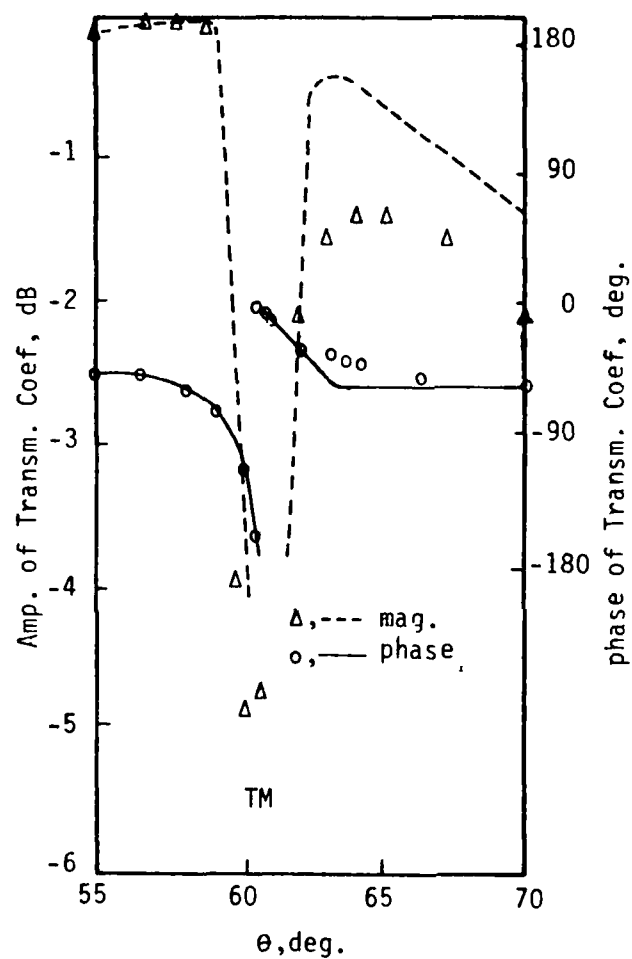


Figure 13. Comparison of the amplitude and phase of the TM transmission coefficient computed by Lee (in lines) and in this research (in triangles and circles) for the case of Figure 12.

are compared. The sharp fall and rise of the transmission coefficient near $\theta=60.6^\circ$ and $\phi=45^\circ$ occurs in both computations. Even though the agreement between $\theta=63^\circ$ and 70° is not quite satisfactory, the excellent agreement exhibited in this important blind-spot phenomenon suggests that the discrepancy is probably not due to program bugs.

Although some of the discrepancies have not been completely resolved, the numerical check is considered satisfactory. Numerical testing for the case of $d_g = 0$ was handicapped by a lack of existing data to compare with. Without other data to guide the initial analysis, it is difficult to perform conclusive numerical checks. Indirect numerical checks were conducted, but they were inefficient, costly, and inconclusive and are not discussed in this report.

SECTION IV

CONCLUSIONS AND RECOMMENDATIONS

Techniques for the analysis of noncanonical microstrip antennas and arrays were investigated with the ultimate goal of antenna performance improvements. There were three major thrusts in this research, each of which culminated in the development of a particular computer program.

The general problem of the radiation of an arbitrary Hertzian dipole, whether horizontal or vertical, electric or magnetic, in general stratified media was numerically solved. The media can have multilayers of various thicknesses with complex dielectric constants. The shortcomings of this approach are that it is not directly applicable to far fields and its convergence depends on the vertical (z) spacing between the dipole and the field points.

The Hertzian dipole algorithm was developed as a basis for the analysis of a general noncanonical microstrip antenna. A method was developed to treat the antenna solely in terms of a horizontal magnetic current along the periphery of the patch. This moment method has several advantages, especially in dealing with microstrip antennas with radial conducting strips. The computer program development encountered difficulties in numerical convergence. Because several new concepts and techniques are involved in this approach, further extensive examinations are needed.

Microstrip array analyses were focused on a monolithic diode-switched screen sandwiched in two dielectric layers. A moment method approach with exponential basis functions was taken. The diode gap region is assumed to have a single mode sinusoidal field distribution. The computer program was tested against data in the literature. Although some excellent agreements were observed, discrepancies also appeared which need further investigation.

This research program is an ambitious endeavor as it deals with difficult electromagnetic and numerical analysis problems. The present accomplishments are expected to contribute to integrated circuits and geophysical science, in addition to microstrip antennas and arrays. For all three major tasks, continued research is recommended for full development and validation of these new techniques.

SECTION V

REFERENCES

1. D. C. Chang, Special Issue Edition on Microstrip Antenna Technology, IEEE Trans. Ant. Prop., Vol AP-29, No. 1, January 1981.
2. I. J. Bahl and P. Bhartia, Microstrip Antennas, Artech House, Dedham, Mass., 1980.
3. J. R. James, P. J. Hall and C. Wood, Microstrip Antenna - Theory and Design, Peter Peregrinus, Stevenage, Herts, England, 1981.
4. R. E. Munson, "Single Slot Cavity Antenna Assembly," U. S. Patent No. 3713162, January 23, 1973.
5. Y. T. Lo, D. Solomon and W. F. Richards, "Theory and Experiment on Microstrip Antennas," IEEE Trans. Ant. Prop., Vol. AP-27, No. 2, pp. 137-145, March 1979.
6. W. C. Chew and J. A. Kong, "Analysis of a Circular Microstrip Disk Antenna with a Thick Dielectric Substrate," IEEE Trans. Ant. Prop., Vol. AP-29, No. 1, pp. 68-76, January 1981.
7. L. C. Shen, "The Elliptical Microstrip Antenna with Circular Polarization," IEEE Trans. Ant. Prop., Vol. AP-29, No. 1, pp. 90-94.
8. S. A. Long, L. C. Shen, D. H. Schanbert, and F. G. Farrar, "An Experimental Study of the Circular-Polarized Elliptical Printed-Circuit Antenna," IEEE Trans. Ant. Prop., Vol. AP-29, No. 1, pp. 95-99, January 1981.
9. K. R. Carver and J. W. Mink, "Microstrip Antenna Technology," IEEE Trans. Ant. Prop., Vol. AP-29, No. 1, pp. 2-24, January 1981.
10. J. F. McIlvenna and N. Kernweis, "Modified Microstrip Disk Antenna Elements," IEE Electrom. Lett., Vol. 15, No. 7, p. 207, 1979.
11. N. Kernweis, and J. F. McIlvenna, "Dual Frequency Microstrip Disc Antenna Elements," RADC Technical Report RADC-TR-79-74, Griffiss AFB, New York, March 1979.
12. P. K. Agrawal and M. C. Bailey, "An Analysis Technique for Microstrip Antennas," IEEE Trans. Ant. Prop., Vol. AP-25, No. 6, pp. 756-759, November 1977.
13. K. R. Carver and E. L. Coffey, "Theoretical Investigation of the Microstrip Antenna," Technical Report, PT-00929, Physical Science Laboratory, New Mexico State University, Las Cruces, N.M., January 1979.

14. G. P. D.S. Cavalcante, D. A. Rogers and A. J. Giarola, "Analysis of Electromagnetic Wave Propagation in Multilayered Media Using Dyadic Green's Functions," Radio Science, Vol. 17, No. 3, pp. 503-308, May-June 1982.
15. J. J. H. Wang, "Computation of Radiation in Stratified Media by Fast Fourier Transform (FFT)," Interim Report RADC-TR-83-140, Rome Air Development Center, Griffiss Air Force Base, NY, September 1983.
16. J. J. H. Wang, "A General Method for the Computation of Radiation in Stratified Media," to be published in Proc. IEE.
17. J. J. H. Wang and C. J. Drane, "Numerical Analysis of Arbitrarily Shaped Bodies Modeled by Surface Patches," IEEE Trans. Microw. Theo. Tech., Vol. MTT-30, No. 8, pp. 1167-1173, August 1982.
18. J. H. Richmond, "Radiation and Scattering by Thin-Wire Structures in the Complex Frequency Domain," ElectroScience Lab., Ohio State University, Columbus, Ohio, Report TR2902-10, July 1973.
19. R. F. Harrington, Field Computation by Moment Method, MacMillan, New York, 1968.
20. A. Farrar and A. T. Adams, "Matrix Methods for Microstrip Three-Dimensional Problems," IEEE Trans. Microw. Theo. Tech., Vol. MTT-20, No. 8, pp. 497-504, August 1972.
21. T. Okoshi and T. Miyoshi, "The Planar Circuit - An Approach to Microwave Integrated Circuitry," IEEE Trans. Microw. Theo. Tech., Vol. MTT-20, No. 4, p. 245-252, April 1972.
22. T. Itoh and R. Mittra, "A New Method for Calculating the Capacitance of a Circular Disk for Microwave Integrated Circuits," IEEE Trans. Microw. Theo. Tech., Vol. MTT-21, pp. 431-432, June 1973.
23. T. Itoh, "Analysis of Microstrip Resonators," IEEE Trans. Microw. Theo. Tech., Vol. MTT-2, No. 11, pp. 946-952, November 1974.
24. R. Chadha and K. C. Gupta, "Green's Functions for Triangular Segments in Planar Microwave Circuits," IEEE Trans. Microw. Theo. Tech., Vol. MTT-28, No. 10, pp. 1139-1143, October 1980.
25. P. C. Sharma and K. C. Gupta, "Desegmentation Method for Analysis of Two-Dimensional Microwave Circuits," IEEE Trans. Microw. Theo. Tech., Vol. MTT-29, No. 10, pp. 1094-1098, October 1981.
26. K. C. Gupta and P. C. Sharma, "Segmentation and Desegmentation Techniques for Analysis of Planar Microstrip Antennas," 1981 IEEE AP Symposium Digest, Los Angeles, pp. 19-22, June 1981.

27. P. C. Sharma and K. C. Gupta, "Optimized Design of Single Feed Circularly Polarized Patch Antennas," 1982 IEEE APS Symposium Digest, Albuquerque, NM, pp. 156-159, May 1982.
28. R. F. Harrington, Time-Harmonic Electromagnetic Fields, McGraw-Hill, New York, 1961.
29. R. J. Mailloux, J. F. McIlvenna, and N. P. Kernweis, "Microstrip Array Technology," IEEE Trans. Ant. Prop., Vol. AP-29, No. 1, pp. 25-37, January 1981.
30. C. C. Liu, J. Shmoys, and A. Hessel, "E-Plane Performance Trade-offs in Two-Dimensional Microstrip-Patch Element Phased Arrays," IEEE Trans. Ant. Prop., Vol. AP-30, No. 6, November 1982.
31. C. C. Chen, "Transmission Through a Conducting Screen Perforated Periodically with Apertures," IEEE Trans. Microw. Theo. Tech., Vol. MTT-18, No. 9, pp. 627-632, September 1970.
32. C. C. Chen, "Diffraction of Electromagnetic Waves by a Conducting Screen Perforated with Circular Holes," IEEE Trans. Microw. Theo. Tech., Vol. MTT-19, No. 5, pp. 475-481, May 1971.
33. S. W. Lee, "Scattering by Dielectric-Loaded Screen," IEEE Trans. Ant. Prop., Vol. AP-19, No. 5, pp. 656-665, September 1971.
34. B. A. Munk, R. G. Kouyoumjian and L. Peters, Jr., "Reflection Properties of Periodic Surfaces by Loaded Dipoles," IEEE Trans. Ant. Prop., Vol. AP-19, No. 5, pp. 612-617, September 1971.
35. B. A. Munk, R. J. Lubbers, and R. D. Fulton, "Transmission Through a Two-Layer Array of Loaded Slots," IEEE Trans. Ant. Prop., Vol. AP-22, pp. 804-809, November 1974.
36. H. H. Ohta, K. C. Lang, C. H. Tsao, and R. Mittra, "Frequency Selective Surface for Satellite Communications Antenna Applications," 1982 IEEE APS Symposium Digest, pp. 475-478, Albuquerque, NM, May 1982.
37. C. A. Chen and C. C. Chen, "Wideband Sharp Frequency Cutoff Dichroic Reflectors for 44/20 GHz Applications," 1982 IEEE APS Symposium Digest, pp. 463-466, Albuquerque, NM, May 1982.
38. J. P. Montgomery, "On the Complete Eigenvalue Solution of Ridged Waveguide," IEEE Trans. Microw. Theo. Tech., Vol. MTT-19, No. 6, pp. 547-555, June 1971.
39. R. Mittra, T. Itoh and T. S. Li, "Analytical and Numerical Studies of the Relative Convergence Phenomenon Arising in the Solution of an Integral Equation by the Moment Method," IEEE Trans. Microw. Theo. Tech., Vol. MTT-20, No. 2, pp. 96-104, February 1972.

40. S. W. Lee, W. R. Jones, and J. J. Campbell, "Convergence of Numerical Solutions of Iris-Type Discontinuity Problems," IEEE Trans. Microw. Theo. Tech., Vol. MTT-19, No. 6, pp. 528-536, June 1971.

APPENDIX A
SOME DEFINITIONS AND RELATIONSHIPS USED
IN SECTION IV

Relationships among the vector potentials are :

$$p_{pq}^{(3)} A_{epq}^{4f} = \delta_p^o \delta_q^o \rho_{pq}^{(1)} A_e^i + \rho_{pq}^{(2)} A_{epq}^r, \quad (A1)$$

$$A_{mpq}^{4f} = \frac{2r_{pq}^{(1)}}{r_{pq}^{(3)}} \left[A_m^i \delta_p^o \delta_q^o \bar{\sigma}_{pq}^{(1)} + A_{mpq}^r \bar{\sigma}_{pq}^{(2)} \right], \quad (A2)$$

$$A_{epq}^{3r} + A_{epq}^{3f} = p_{pq}^{(3)} A_{epq}^{4f}, \quad (A3)$$

$$-A_{mpq}^{3r} + A_{mpq}^{3f} = \bar{\sigma}_{pq}^{(3)} A_{mpq}^{4f}, \quad (A4)$$

$$A_{epq}^{2r} + A_{epq}^{2f} = \delta_p^o \delta_q^o \rho_{pq}^{(1)} A_e^i + \rho_{pq}^{(2)} A_{epq}^r, \quad (A5)$$

$$A_{mpq}^{2r} - A_{mpq}^{2f} = -\delta_p^o \delta_q^o \bar{\sigma}_{pq}^{(1)} A_m^i - \bar{\sigma}_{pq}^{(2)} A_{mpq}^r. \quad (A6)$$

Propagation and dielectric parameters are:

$$\gamma_{pq} = [k_o^2 - (U_{po}^2 + V_{pq}^2)]^{1/2}, \quad (A7)$$

$$\epsilon_{pq} = [k_o^2 \epsilon_1 - (U_{po}^2 + V_{pq}^2)]^{1/2}, \quad (A8)$$

$$\epsilon_{pq} = [k_o^2 \epsilon_2 - (U_{po}^2 + V_{pq}^2)]^{1/2}, \quad (A9)$$

$$\begin{aligned} \left. \begin{aligned} \gamma_{pq}^{(1)} \\ \gamma_{pq}^{(1)} \end{aligned} \right\} &= \exp(j\gamma_{pq} \tau_1) \frac{\gamma_{pq} + \gamma_{pq}}{2\gamma_{pq}} \\ &\quad \left[\exp(-j\gamma_{pq} \tau_1) \pm \frac{\gamma_{pq} - \gamma_{pq}}{\gamma_{pq} + \gamma_{pq}} \exp(+j\gamma_{pq} \tau_1) \right], \end{aligned} \quad (A10)$$

$$\left. \begin{array}{l} \rho_{pq}^{(2)} \\ \sigma_{pq}^{(2)} \end{array} \right\} = \exp(j\gamma_{pq}\tau_1) \frac{\alpha_{pq} + \gamma_{pq}}{2\alpha_{pq}} \left[\pm \exp(+j\alpha_{pq}\tau_1) \pm \frac{\alpha_{pq} - \gamma_{pq}}{\alpha_{pq} + \gamma_{pq}} \exp(-j\alpha_{pq}\tau_1) \right], \quad (A11)$$

$$\left. \begin{array}{l} \bar{\rho}_{pq}^{(1)} \\ \bar{\sigma}_{pq}^{(1)} \end{array} \right\} = \exp(j\gamma_{pq}\tau_1) \frac{\alpha_{pq} + \epsilon_1 \gamma_{pq}}{2\alpha_{pq}} \left[\exp(-j\alpha_{pq}\tau_1) \pm \frac{\alpha_{pq} - \epsilon_1 \gamma_{pq}}{\alpha_{pq} + \epsilon_1 \gamma_{pq}} \exp(j\alpha_{pq}\tau_1) \right], \quad (A12)$$

$$\left. \begin{array}{l} \bar{\rho}_{pq}^{(2)} \\ \bar{\sigma}_{pq}^{(2)} \end{array} \right\} = \exp(-j\gamma_{pq}\tau_1) \frac{\alpha_{pq} + \epsilon_1 \gamma_{pq}}{2\alpha_{pq}} \left[\pm \exp(+j\alpha_{pq}\tau_1) \pm \frac{\alpha_{pq} - \epsilon_1 \gamma_{pq}}{\alpha_{pq} + \epsilon_1 \gamma_{pq}} \exp(-j\alpha_{pq}\tau_1) \right], \quad (A13)$$

$$\left. \begin{array}{l} \rho_{pq}^{(3)} \\ \sigma_{pq}^{(3)} \end{array} \right\} = \exp(-j\gamma_{pq}\tau_2) \frac{\beta_{pq} + \gamma_{pq}}{2\beta_{pq}} \left[\exp(+j\beta_{pq}\tau_2) \pm \frac{\beta_{pq} - \gamma_{pq}}{\beta_{pq} + \gamma_{pq}} \exp(-j\beta_{pq}\tau_2) \right], \quad (A14)$$

$$\left. \begin{array}{l} \bar{\rho}_{pq}^{(3)} \\ \bar{\sigma}_{pq}^{(3)} \end{array} \right\} = \exp(-j\gamma_{pq}\tau_2) \frac{\beta_{pq} + \epsilon_2\gamma_{pq}}{2\beta_{pq}} \left[\exp(+j\beta_{pq}\tau_2) \pm \frac{\beta_{pq} - \epsilon_2\gamma_{pq}}{\beta_{pq} + \epsilon_2\tau_{pq}} \exp(-j\beta_{pq}\tau_2) \right]. \quad (A15)$$

The integral equations are

$$\begin{aligned} & \int dx' dy' \psi_{pq}(x, y) \psi_{pq}^*(x', y') \{ E_{ax} [(U_{po} D_{pq}) (-V_{pq}) + (V_{pq} E_{pq}) (U_{po})] \\ & + E_{ay} [(U_{po} D_{pq}) (U_{po}) + (V_{pq} E_{pq}) (V_{pq})] \} \\ & = \{ A_e^i U_{oo} \frac{\alpha_{oo} [\sigma_{oo}^{(2)} \rho_{oo}^{(1)} - \sigma_{oo}^{(1)} \rho_{oo}^{(2)}]}{k_o \rho_{oo}^{(2)}} \\ & + A_m^i \eta_o V_{oo} \frac{\bar{\sigma}_{oo}^{(2)} \bar{\rho}_{oo}^{(1)} - \bar{\sigma}_{oo}^{(1)} \bar{\rho}_{oo}^{(2)}}{\bar{\sigma}_{oo}^{(2)}} \} \psi(x, y)_{oo}, \end{aligned} \quad (A16)$$

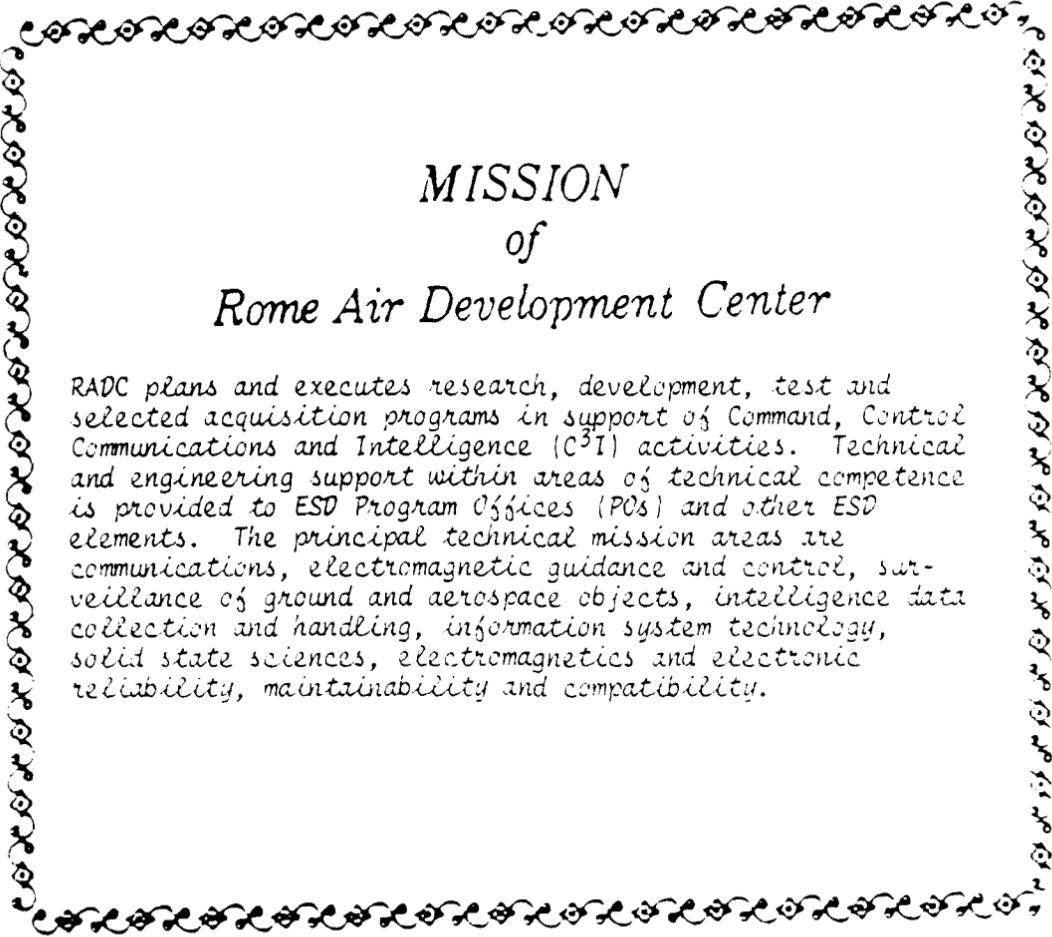
and

$$\begin{aligned} & \int dx' dy' \psi_{pq}(x, y) \psi_{pq}^*(x', y') \{ E_{ax} [(V_{po} D_{pq}) (-V_{pq}) + (-U_{po} E_{pq}) (U_{po})] \\ & + E_{ay} [(V_{pq} D_{pq}) (U_{po}) + (-U_{po} E_{pq}) (V_{pq})] \} \\ & = \{ A_p^i V_{oo} \frac{\alpha_{oo} [\sigma_{oo}^{(2)} \rho_{oo}^{(1)} - \sigma_{oo}^{(1)} \rho_{oo}^{(2)}]}{k_o \rho_{oo}^{(2)}} \\ & - A_m^i \eta_o U_{oo} \frac{\bar{\sigma}_{oo}^{(2)} \bar{\rho}_{oo}^{(1)} - \bar{\sigma}_{oo}^{(1)} \bar{\rho}_{oo}^{(2)}}{\bar{\sigma}_{oo}^{(2)}} \} \psi(x, y)_{oo}. \end{aligned} \quad (A17)$$

where,

$$D_{pq} = \frac{j(\alpha_{pq\sigma}^{(2)} \rho_{pq}^{(3)} - \beta_{pq\sigma}^{(3)} \rho_{pq}^{(2)})}{k_o \rho_{pq}^{(2)} \rho_{pq}^{(3)} (U_{pq}^2 + V_{pq}^2)} \quad (A18)$$

$$E_{pq} = \frac{jk_o(\epsilon_{1r} \beta_{pq\bar{\sigma}}^{(2)} \bar{\rho}_{pq}^{(3)} - \epsilon_{2r} \alpha_{pq\bar{\sigma}}^{(3)} \bar{\rho}_{pq}^{(2)})}{\alpha_{pq\beta} \bar{\rho}_{pq}^{(2)} \bar{\rho}_{pq}^{(3)} (U_{pq}^2 + V_{pq}^2)} \quad (A19)$$



*MISSION
of
Rome Air Development Center*

RADC plans and executes research, development, test and selected acquisition programs in support of Command, Control Communications and Intelligence (C³I) activities. Technical and engineering support within areas of technical competence is provided to ESD Program Offices (POs) and other ESD elements. The principal technical mission areas are communications, electromagnetic guidance and control, surveillance of ground and aerospace objects, intelligence data collection and handling, information system technology, solid state sciences, electromagnetics and electronic reliability, maintainability and compatibility.

END

FILMED

5-85

DTIC

